

THE YOUNGEST KNOWN X-RAY BINARY: CIRCINUS X-1 AND ITS NATAL SUPERNOVA REMNANT

S. HEINZ¹, P. SELL¹, R.P. FENDER^{2,3}, P.G. JONKER^{4,5,6}, W.N. BRANDT⁷, D.E. CALVELO-SANTOS³, A.K. TZIOUMIS⁸,
M.A. NOWAK⁹, N.S. SCHULZ⁹, R. WIJNANDS¹⁰, AND M. VAN DER KLIS¹⁰

Draft version December 4, 2013

Abstract

Because supernova remnants are short lived, studies of neutron star X-ray binaries within supernova remnants probe the earliest stages in the life of accreting neutron stars. However, such objects are exceedingly rare: none were known to exist in our Galaxy. We report the discovery of the natal supernova remnant of the accreting neutron star Circinus X-1, which places an upper limit of $t < 4,600$ years on its age, making it the youngest known X-ray binary and a unique tool to study accretion, neutron star evolution, and core collapse supernovae. This discovery is based on a deep 2009 *Chandra* X-ray observation and new radio observations of Circinus X-1. Circinus X-1 produces type I X-ray bursts on the surface of the neutron star, indicating that the magnetic field of the neutron star is small. Thus, the young age implies either that neutron stars can be born with low magnetic fields or that they can rapidly become de-magnetized by accretion. Circinus X-1 is a microquasar, creating relativistic jets which were thought to power the arcminute scale radio nebula surrounding the source. Instead, this nebula can now be attributed to non-thermal synchrotron emission from the forward shock of the supernova remnant. The young age is consistent with the observed rapid orbital evolution and the highly eccentric orbit of the system and offers the chance to test the physics of post-supernova orbital evolution in X-ray binaries in detail for the first time.

Subject headings: stars: binaries — stars: neutron — stars: individual (Circinus X-1) — ISM: supernova remnants — X-rays: binaries

1. INTRODUCTION

Observations of young high-mass X-ray binary (HMXB) neutron stars can provide powerful constraints on the physics of accretion, supernova explosions and the early evolution and birth properties of neutron stars. Important properties that can be constrained from observations of such systems include the age, the magnetic field strength, and the spin of a newly born neutron star, the mass of the neutron star, the mass of its progenitor star, the mass of its companion star, supernova kick velocities, and the pre- and post-supernova orbital parameters of the binary system and their evolution.

Identifying newly formed HMXBs requires the detection of the supernova remnant in which they formed, which allows an accurate determination of their age. This motivates the search for supernova remnants around Galactic HMXBs. However, the time during which the

remnant is visible is at least three orders of magnitude shorter than typical binary and stellar evolution time scales, making X-ray binaries within their remnants extremely rare objects. The only firmly established X-ray binary within a supernova remnant in our Galaxy, the X-ray binary SS433 (Geldzahler et al. 1980), most likely does not contain a neutron star but a black hole.

The neutron star¹¹ X-ray binary Circinus X-1 has historically been among the brightest X-ray sources in the sky. The often erratic accretion behavior, the unusually powerful jets of this microquasar, the difficulty in identifying the mass and type of the companion star, and the large scale radio nebula historically thought to be produced by the jets (Stewart et al. 1993; Tudose et al. 2006) have made it hard to classify the source in the context of typical neutron star X-ray binary classification schemes (e.g. Oosterbroek et al. 1995; Calvelo et al. 2012b). The source has often been referred to as a low-mass X-ray binary, which would imply an old age for Circinus X-1, but many of its characteristics suggest that the source might, in fact, be very young (Clarkson et al. 2004; Jonker et al. 2007).

Circinus X-1's large X-ray flux has made searches for faint diffuse X-ray emission around the source all but impossible, because the X-ray light from the neutron star is scattered into an arcminute scale halo by interstellar dust, easily overwhelming any underlying low surface brightness emission. In this paper, we present the discovery of the supernova remnant of the neutron star X-ray binary Circinus X-1.

Literature estimates for the distance to Circinus X-1

heinzs@astro.wisc.edu

¹ Department of Astronomy, University of Wisconsin-Madison, Madison, WI 53706, USA

² University of Oxford, Astrophysics, Oxford OX1 3RH, UK

³ Physics and Astronomy, University of Southampton, Highfield, Southampton SO17 1BJ, UK

⁴ SRON, Netherlands Institute for Space Research, 3584 CA, Utrecht, the Netherlands

⁵ Department of Astrophysics/IMAPP, Radboud University Nijmegen, 6500 GL, Nijmegen, The Netherlands

⁶ Harvard-Smithsonian Center for Astrophysics, Cambridge, MA 02138, USA

⁷ Department of Astronomy & Astrophysics, The Pennsylvania State University, University Park, PA 16802, USA

⁸ Australia Telescope National Facility, CSIRO, Epping, NSW 1710, Australia

⁹ Kavli Institute for Astrophysics and Space Research, Massachusetts Institute of Technology, Cambridge, MA 02139, USA

¹⁰ Astronomical Institute “Anton Pannekoek”, University of Amsterdam, 1090 GE Amsterdam, The Netherlands

¹¹ The unambiguous identification of Circinus X-1 as a neutron star is based on the detection of type I X-ray bursts from the source (Tennant et al. 1986; Linares et al. 2010)

range from 4 kpc (Iaria et al. 2005) to 11 kpc, with a most likely value of $D = 8 - 10.5$ kpc (based on both the radius-expansion burst method and the observed Galactic neutral Hydrogen column density, Jonker & Nelemans 2004). Throughout this paper, we will use a fiducial distance of $D = 8d_8$ kpc to the source, with explicit dependence of all numerical values on the true distance expressed in terms of d_8 . The qualitative results presented in this paper are insensitive to the actual value of d_8 .

2. OBSERVATIONS

2.1. Data Reduction and Image Analysis

Circinus X-1 entered an extended period of low flux in about 2005, which allowed the detection of extended X-ray synchrotron emission from the powerful jets of this microquasar (Heinz et al. 2007; Soleri et al. 2009). We re-observed the source for 98,723 seconds with the Advanced CCD Imaging Spectrometer on *Chandra* on May 1, 2009¹² to confirm this detection and study the jet emission while the source was at the lowest flux state ever recorded. Data were taken in timed exposure mode and telemetered in Faint mode. The data were reprocessed, reduced, and analyzed using CIAO version 4.5, CALDB version 4.5.6, and XSPEC version 12.8.0.

An analysis of the jet emission was presented in a previous paper (Sell et al. 2010). This analysis did not address the large scale diffuse X-ray emission beyond the synchrotron jets in detail, which was tentatively interpreted as emission from the dust scattering halo. Below, we present a full investigation of the arcminute scale diffuse emission, showing clearly that the emission is, in fact, not due to dust scattering.

Careful inspection of the faint, diffuse emission in observation Obs ID 10062 beyond the synchrotron jets reveals a smooth, roughly circular X-ray nebula, shown in Fig. 1, that extends about 2.5 arcminutes from the point source, beyond which the emission shows a well defined edge in the Northern half of the image (the Southern half is not fully covered by the CCDs). In order to visualize the low surface-brightness excess, we applied adaptive binning to the image, using weighted Voronoi-Delaunay tessellation with a minimum signal-to-noise of 4 per resolution element (wvt image, see Diehl & Statler 2006) and smoothed the resulting image using a Gaussian with a FWHM of 10 *Chandra ACIS* pixels.

2.2. Eliminating Dust Scattering

Dust scattering of emission from the bright, central accreting neutron star source could in principle produce diffuse emission on the scales of the observed nebula. Dust scattering can be ruled out as the dominant source of the extended X-ray emission in Obs ID 10062 on three grounds: (a) Given historical observations of the dust scattering halo of Circinus X-1, the X-ray nebula is too bright to be due to dust scattering, (b) the X-ray spectrum of the nebula is inconsistent with the expected powerlaw emission of the dust scattering halo, and (c) a chance coincidence of the close morphological correspondence between the X-ray and radio nebulae is highly unlikely. We will discuss these arguments in turn.

¹² Obs ID 10062 in the *Chandra* archive

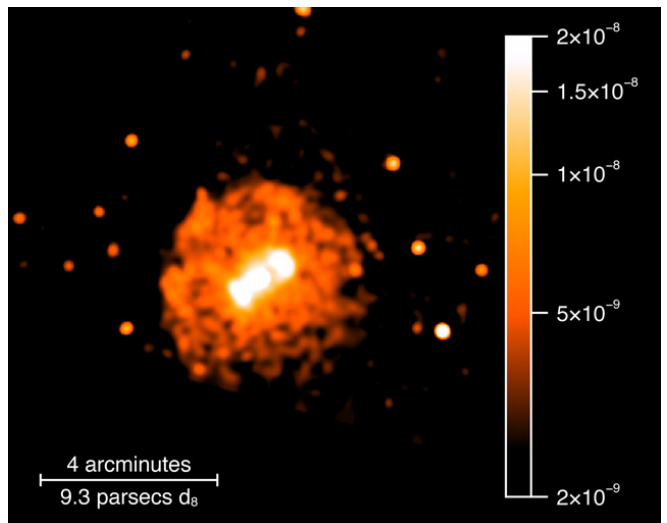


FIG. 1.— *Chandra* X-ray image of the supernova remnant and jet of Circinus X-1 in the energy range 1-3 keV. Adaptive binning to a signal-to-noise of 4 per resolution element and Gaussian smoothing with 10 pixel FWHM were applied for noise reduction. The CCD read-out streak was removed from the image according to standard practices. The central elongated brightness enhancement (yellow-white color) is due to the neutron star point source and the bi-polar jet emission (Heinz et al. 2007; Soleri et al. 2009; Sell et al. 2010). The scale bar shows an angular scale of 4 arcminutes. The color bar shows the surface brightness scale in units of photons $s^{-1} cm^{-2} arcsec^{-2}$. The image is oriented such that North is up and East is to the Left.

2.2.1. Surface Brightness Arguments Against Dust Scattering

The central brightness enhancement in Fig. 1 is due to the neutron star point source and the bi-polar jet emission. However, the emission flattens at radii between 30 and 150 arcseconds, deviating from the expected, gradually declining, radial brightness profile of dust scattering.

In order to eliminate dust scattering as the source of the extended emission, we constructed radial surface brightness profiles Σ of the dust scattering halo from two previous *Chandra* observations (Obs ID 706, March 2000; Obs OD 1700, June 2000), shown in Fig. 2. During these observations, the X-ray binary point source was a factor of approximately 2,500 and 1,000 brighter than during Obs ID 10062, respectively. Given these high fluxes and the existing estimate of the dust scattering fraction for Circinus X-1 (Predehl & Schmitt 1995), any extended emission beyond the inner few arcseconds in Obs ID 706 and Obs ID 1700 must be due to dust scattering.

Dust scattering induces a time delay of $\Delta t = 1.1 d_8 \text{ days} (\theta/100'')^2 x / (1-x)$ between the arrival of light from the point source and the arrival of the corresponding scattered dust emission (Predehl & Klose 1996) where θ is the angle of the scattering halo on the sky and x is the fractional distance from the observer to the dust. We must therefore consider the point source emission not just during the observation but also during the days leading up to each observation.

The X-ray lightcurves for the two weeks prior to each of the three observations are shown in Fig. 3. The daily average *Rossi X-ray Timing Explorer All Sky Monitor (ASM)* flux for Circinus X-1 in the two weeks prior to Obs ID 706 was approximately constant at ≈ 80 counts per second. The analysis of the point source and the dust

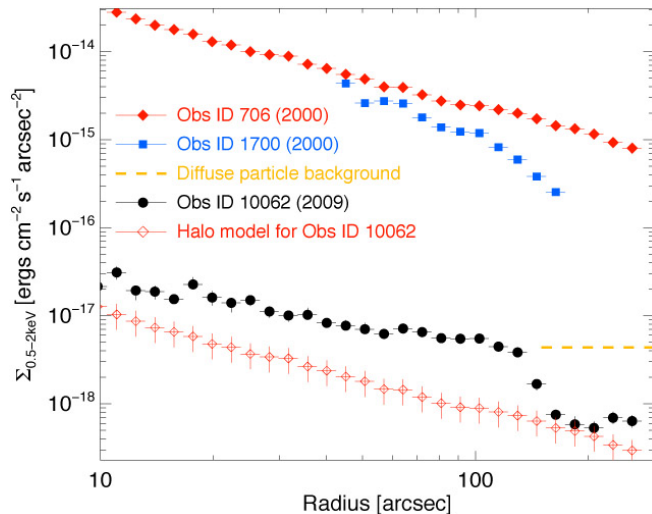


FIG. 2.— The 0.5-2 keV X-ray surface brightness Σ of *Chandra* observations Obs ID 706, 1700, and 10062 shown as solid red diamonds, blue squares, and black dots, respectively, plotted against radial distance from Circinus X-1. Diffuse particle background emission at a uniform level of $\Sigma_{0.5-2.0} \sim 4.4 \times 10^{-18} \text{ ergs s}^{-1} \text{ cm}^{-2} \text{ arcsec}^{-2}$ was subtracted from the Obs ID 10062 profile (shown as dashed yellow line for comparison). Regions dominated by synchrotron jet emission were excluded. The estimated contribution from the dust scattering halo to Obs ID 10062 is shown as open red diamonds, well below the measured surface brightness of the supernova remnant. Vertical error bars indicate one-sigma uncertainties.

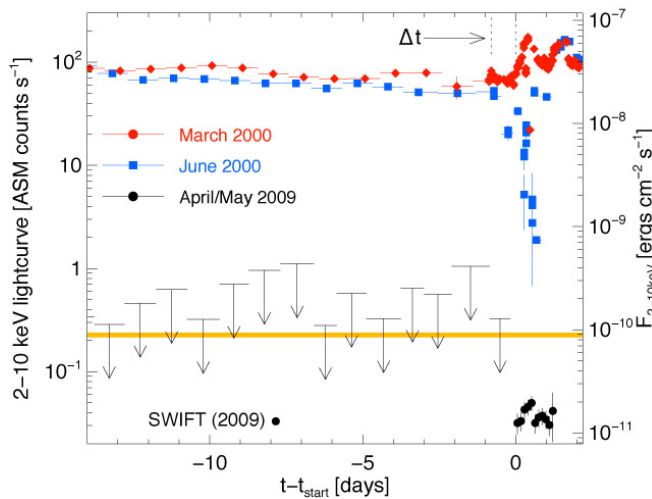


FIG. 3.— X-ray lightcurves of Circinus X-1. *Rossini X-ray Timing Explorer All Sky Monitor* lightcurves of the point source emission from Circinus X-1 during the time interval $t_{\text{start}} - 14$ days to $t_{\text{start}} + 2$ days, measured from the start times t_{start} of Obs IDs 706, 1700, and 10062 (red diamonds, blue squares, and black upper limits, respectively). The *Chandra* and *Swift* fluxes during and before Obs ID 10062 are shown as black dots. The inferred dust-delay time for the outer halo of $\Delta t \lesssim 1$ day is shown by the horizontal arrow. The yellow horizontal bar indicates the point source flux required to produce a halo as bright as the nebula in Obs ID 10062. Vertical error bars and upper limits indicate one-sigma uncertainties. There is no indication from the observations that the source could have been bright enough just prior to *Chandra* Obs ID 10062 to produce the observed nebula by dust scattering.

scattering halo was restricted to the first 40% of Obs ID 706, representative of the flux the source had in the two weeks leading up to Obs ID 706, avoiding the bright flare during the second half of the observation visible in Fig. 3.

From the dust scattering emission in Obs ID 706, we constructed the expected radial surface brightness profile of the dust scattering contribution to Obs ID 10062, using the ratio of the 0.5-2.0 keV point source fluxes of 2720 measured with *Chandra* for both observations (open red diamonds in Fig. 2; error bars account for the variability of the source in the week leading up to Obs ID 706, estimated from the standard deviation of the orbit-to-orbit ASM flux variations, propagated in quadrature with the uncertainties in the radial surface brightness profile of Obs ID 706 and the point source flux of Obs ID 10062.

The radial surface brightness profile for Obs ID 10062 itself, excluding the regions of the image identified as synchrotron shock emission (Sell et al. 2010), is shown as black dots in Fig. 2. Over the extent of the nebula, the observed surface brightness in the 0.5-2 keV energy band is a factor of approximately 3 to 6 higher than the predicted contribution from the dust scattering halo. Thus, the nebula cannot have been produced by dust scattering while the point source flux was at the level measured *during* our *Chandra* observation.

Using Obs ID 1700, we can estimate the delay time Δt for the dust towards Circinus X-1 to show the nebula in Obs ID 10062 cannot have been produced by a flare of the point source *prior* to Obs ID 10062: In the two weeks prior to Obs ID 1700, the *ASM* X-ray lightcurve of Circinus X-1 was roughly constant at 50-70 counts per second, close the flux before Obs ID 706. One day before Obs ID 1700, the *ASM* source flux dropped sharply to 10-20 counts/s and then re-brightened to approximately 30 counts per second during the *Chandra* observation.

The halo surface brightness within the inner 100 arcseconds of Obs ID 1700 is at roughly 50% of the halo surface brightness in Obs ID 706, approximately the same ratio as the point source fluxes during the observations. Outward of 100 arcseconds, the halo brightness drops steeply in Obs ID 1700 to about 10%-20% of the surface brightness in the outer halo of Obs ID 706. In the two week intervals leading up to both observations, the *only* time period before Obs ID 1700 when the point source was a factor of 5 to 10 dimmer than it was at the corresponding time before Obs ID 706 was during the 24 hours leading up to the observations. Thus, the dust delay time for annuli between 100 and 170 arcseconds from the central source must be $\Delta t \leq 1$ day, and correspondingly shorter on smaller angular scales.

During the second half of Obs ID 706, the dust scattering halo shows a $\sim 25\%$ increase in flux, roughly within 10,000 seconds of the point source brightening. This yields an independent estimate of $\Delta t \sim 0.4$ days for the variability and thus the dust delay time of the halo, consistent with the estimate of $\Delta t \leq 1$ day from Obs ID 1700.

On the other hand, the X-ray nebula in Obs ID 10062 shows no sign of X-ray variability in any of the annuli between 20 and 150 arcseconds, consistent with the expectation for diffuse emission from an astrophysical source like a supernova remnant, but inconsistent with dust scattering from a bright flare of the point source during the time leading up to the observation. We can place an

upper limit on any secular change of the surface brightness during the observation of less than 2.5% per day.

Obs ID 10062 had an exposure time longer than 1 day, and the point source flux during that observation was constant within the uncertainties.

2.2.2. Spectral Evidence Against Dust Scattering

The X-ray spectrum of the nebula shows clear evidence for emission lines from Magnesium, Silicon, and Sulfur (see §2.5 for a detailed discussion of the spectrum). On the other hand, the point source spectrum is best fit by a powerlaw $F_\nu \propto \nu^{0.4}$, modified by photoelectric absorption. Dust scattering is expected to steepen this powerlaw by a factor of ν^{-2} . The resulting powerlaw spectrum is statistically inconsistent with the observed thermal nebular spectrum. It is consistent with the residual background emission in the annuli beyond the nebula, indicating that residual dust scattering emission is present at the low level predicted by the profile derived from Obs ID 706.

2.2.3. Morphological Evidence Against Dust Scattering

Finally, and most importantly, the sharp edge of the northern half of the X-ray nebula closely follows the edge of the radio nebula (Fig. 5), including several deviations from the generally circular shape of the northern hemisphere and the east-west asymmetry that would not be expected for an axi-symmetric dust scattering halo. It is highly unlikely that two independent mechanisms (dust scattering and the shock responsible for the radio emission) would produce such a close match between these two shapes.

We conclude that the bulk of the extended emission in Obs ID 10062 cannot be caused by dust scattering.

2.3. ATCA Radio Observations

We obtained a high-resolution radio image of the remnant in the 1.1-3.1 GHz band, taken with the Australia Telescope Compact Array on December 16, 2011, with an integration time of 19.5 hours in 6A array configuration (minimum baseline of 337m, maximum of 5939m). The FWHM beam size of the image is 4.9×4.0 arcsec at position angle 0.5° , with a theoretical rms noise of $4\mu\text{Jy}$ per beam. PKS1511-55 was used for flux, phase, and band-pass calibration.

Deconvolution was carried out using a combination of the MFCLEAN (Sault & Wieringa 1994) and CLEAN (Högbom 1974) subroutines. Data processing was carried out in MIRIAD (Sault et al. 1995).

Previous radio observations of the nebula were taken at lower resolution (Stewart et al. 1993; Tudose et al. 2006), suffering from contamination of the large scale diffuse emission by the bright jet and point source emission. Higher resolution images of Circinus X-1, taken to investigate the sub-arcsecond jet emission close to the point source typically over-resolve the diffuse emission, but recent 5.5 GHz observations show evidence for a sharp, filamentary edge to the nebula (Calvelo et al. 2012b).

The radio image presented here clearly resolves the nebula as an edge-brightened, asymmetric synchrotron shell, shown in Fig. 4. Figure 5 shows an overlay of this radio image on the diffuse X-ray emission. The portions of the nebula covered by the *Chandra* CCDs line up well

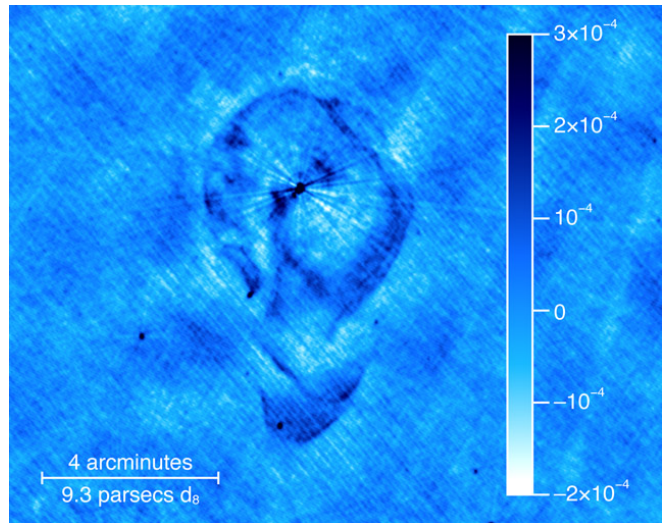


FIG. 4.— 1.1-3.1 GHz broad band radio image of the Circinus X-1 supernova remnant and jet taken with the Australia Compact Telescope Array on 16 December 2011. The scale bar shows an angular scale of 4 arcminutes. The color bar shows the image surface brightness in units of Jy per beam, with a FWHM beam size of 4.9×4.0 arcseconds at position angle 0.5° . The image is oriented such that North is up and East is to the Left.

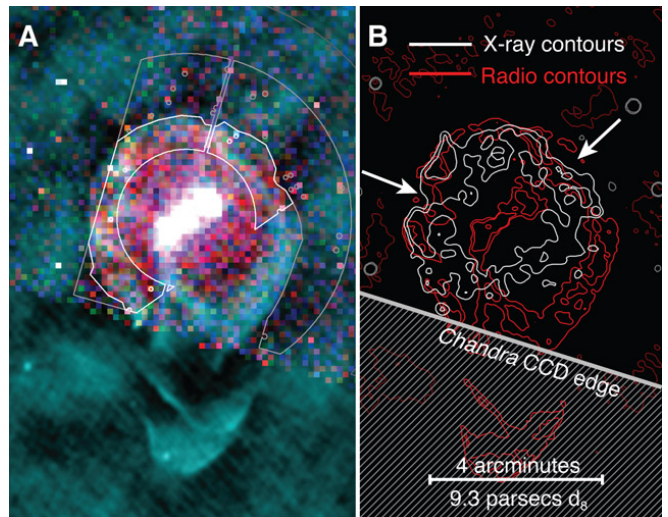


FIG. 5.— Radio-X-Ray Overlay of the Circinus X-1 Supernova Remnant. *Left panel A*: soft 1-2 keV, medium 2-3 keV, and hard 3-5 keV X-ray emission in red, green, and blue, respectively; the radio synchrotron emission is overlaid in Cyan. The extraction regions for the source spectrum and the inner background spectrum are indicated as white and light-gray contours, respectively. The inner rim of the outer background extraction region can be seen as the dark-gray contour. *Right panel B*: overlay of the radio (red) and X-ray (white) contours of the remnant edge. Contours we identify as part of the remnant are shown in a lighter shade. The part of the image not covered by the *Chandra* CCDs is marked by the grey hatched area. The white arrows indicate dents where both radio and X-ray emission deviate from a simple circular contour. The images are oriented such that North is up and East is to the Left.

with the radio nebula: The edge of the X-ray emission is just inside the radio shell, even following a pronounced dent in the North-Western section of the radio image. The morphology of both the X-ray and the radio images are consistent with the expected appearance of a young supernova remnant.

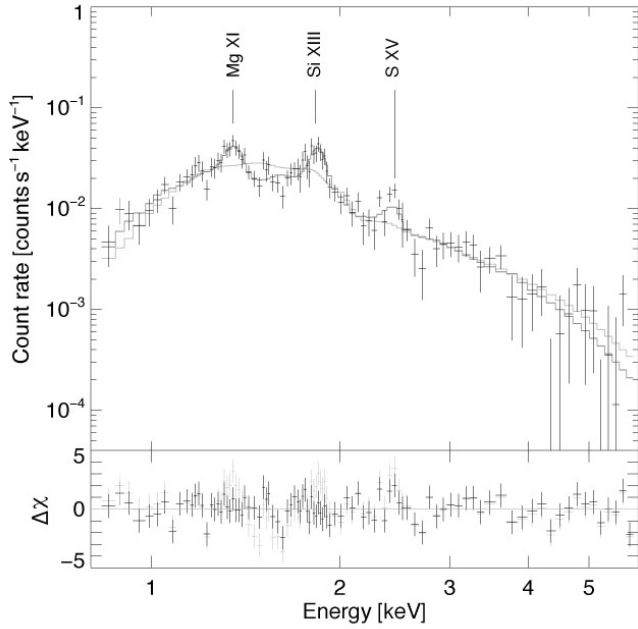


FIG. 6.— *Chandra Top panel*: X-ray Spectrum of the outer portion of the supernova remnant, showing Magnesium XI and XII (1.4 keV), Silicon XIII (1.8 keV) and Sulfur XV (2.4 keV) emission lines. Error bars indicate one-sigma uncertainties. The dark gray histogram shows the best fit SEDOV shock model with photoelectric foreground absorption, the light-grey histogram shows the best-fit powerlaw model. The spectrum contains approximately 2900 net source counts and covers approximately 30% of the remnant area visible on the ACIS CCDs. *Bottom panel*: fit residuals for the best fit SEDOV and powerlaw models in dark and light grey, respectively.

2.4. Extraction of the Remnant X-ray Spectrum:

Because of the potential contamination by residual emission from the dust scattering halo, we used only the outer portion of the remnant beyond 95 arcseconds from the source, where the fractional contribution from dust scattering should be smallest, to determine the remnant spectrum. We restricted the spectral extraction to the northern portion of the nebula, where the surface brightness of the nebula and therefore the signal-to-noise is largest. This section of the nebula is fully covered by the *ACIS S-3 CCD*. Point sources, the read-out streak, and regions affected by the dithered edge of the *ACIS S-3* chip were excluded from the extraction.

We chose the primary background region to be close to the remnant in order to model potential residual emission from the dust scattering halo. A second background region on the farthest corner of the same *Chandra ACIS S-3 CCD* was chosen to subtract the particle background. The resulting spectrum contains approximately 2900 net source counts in the 0.8-6 keV range used for the fits, out of 7774 total (source plus background) counts. The background-subtracted spectrum used in the fits is shown in Fig. 6. The source and inner background extraction regions are indicated in Fig. 5.

From the radial surface brightness profile of the halo, we estimate the maximum contamination by dust scattering to be $< 20\%$ of the 0.5-3 keV flux from the remnant. We modeled this contribution by jointly fitting a powerlaw modified by photoelectric absorption to both the remnant and the primary background region, in addition to the Sedov blast wave model, which we fitted to

the remnant spectrum only.

The relative flux ratio of the halo emission contaminating the spectrum of the remnant to the halo emission in the primary background spectrum was derived from the radial surface brightness profile of the dust scattering halo in Obs ID 706 derived in the appendix and shown in Fig. 2, integrated over the regions from which the spectra were extracted. Particle background contamination (subtracted from the spectrum using the second background region) dominates the spectrum above energies of 6 keV and below energies of 0.8 keV, which motivated the choice of the energy band of 0.8 to 6 keV used in the fits in §2.5.

2.5. Spectral Fits

The X-ray spectrum of the nebula, shown in Fig. 6, clearly indicates significant photoelectric attenuation by foreground gas and dust. The interstellar neutral hydrogen column density of $N_{\text{H}} \approx 1.8 \pm 0.1 \times 10^{22} \text{ cm}^{-2}$ determined from the spectral fits¹³ is consistent with a source distance of $D \approx 8 \text{ kpc}$ (Jonker & Nelemans 2004). The large column density is consistent with previous estimates and the large amount of visible extinction towards Circinus X-1.

The X-ray spectrum shows clear evidence for emission lines from Magnesium, Silicon, and Sulfur, inconsistent with a simple powerlaw model, which would be expected if the X-rays were due to synchrotron emission. Figure 6 shows the best fit powerlaw model and residuals in the top and bottom panels, respectively. With a reduced chi-square of $\chi_{\text{red, power}}^2 = \frac{197.63}{91 \text{ d.o.f.}} = 2.2$, we can formally rule out a powerlaw model for the X-ray spectrum with a high degree of confidence. Adding narrow Gaussian emission lines for Magnesium, Silicon, and Sulfur improves the chi-square by $\Delta\chi_{\text{Mg}}^2 = 30.27$, $\Delta\chi_{\text{Si}}^2 = 36.31$, and $\Delta\chi_{\text{S}}^2 = 24.58$, respectively.

On the other hand, non-equilibrium shock models such as PSHOCK, NEI, and SEDOV provide a statistically satisfactory spectral fit, with a reduced chi-square of $\chi_{\text{red, non-eq}}^2 = 1.0$ in all three cases, consistent with the expectations for a young supernova remnant. Non-equilibrium models are statistically preferred over equilibrium ionization models like APEC, which give a best-fit reduced chi-square of $\chi_{\text{red, eq}}^2 = 1.2$.

Based on the evidence from both imaging and spectral analysis, we conclude that the X-ray nebula must be the supernova remnant of Circinus X-1. We estimate the supernova parameters by fitting the spectrum with a SEDOV blast wave model (Hamilton et al. 1983; Borkowski et al. 2001). The best fit model is shown as in black in Fig. 6. Fit results are listed in Table 1 and confidence intervals of the key supernova parameters derived from the SEDOV model fits are plotted in Fig. 7.

The formal best fit shock temperature is $T_s = 1.0_{-0.4}^{+7.3} \text{ keV}$, corresponding to a shock velocity of $v_s = 910_{-210}^{+1690} \text{ km s}^{-1}$ and a remnant age of $t = 2440_{-1590}^{+720} \text{ d}_8 \text{ yrs}$. The dynamical remnant parameters, such as the age, the swept up mass, and the explosion energy, are derived from the spectral fits using the standard relations for adiabatic supernova remnants in the

¹³ Uncertainties are quoted at the one-sigma 68% confidence level unless otherwise specified

TABLE 1
PHABS*SEDOV BEST FIT PARAMETERS^a.

$N_{\text{H},22}^{\text{b}}$	T_e^{c}	T_s^{d}	Z/Z_{\odot}^{e}	τ_{11}^{f}	$EM_{\text{L},17}^{\text{g}}$
1.8 ± 0.1	$0.9^{+0.4}_{-0.8}$	$1.07^{+0.3}_{-0.4}$	$1.3^{+0.9}_{-0.5}$	$1^{+1}_{-0.2}$	$1.5^{+1.3}_{-0.7}$

^a The reduced chi-square of the best fit parameters shown in the table is $\chi^2/\text{d.o.f.} = 348.5/345$.

^b Absorption column density $N_{\text{H},22} \equiv N/10^{22} \text{ cm}^{-2}$ in units of 10^{22} cm^{-2}

^c Electron temperature T_e in keV

^d Shock temperature T_s in keV

^e Metal abundance Z in units of solar metallicity Z_{\odot}

^f Ionization age $\tau_{11} \equiv \tau/10^{11} \text{ s}$ in units of 10^{11} s , where $\tau = n_e t$ is the product of the electron density n_e behind the shock and the age of the remnant t

^g Spectral normalization, given as the line emission measure $EM_{\text{L}} = \int dn_e n_{\text{H}}$, averaged over the spectral extraction region, in units of 10^{17} cm^{-5}

Sedov expansion phase (Hamilton et al. 1983, equations 4a-4e; see also, e.g., Safi-Harb et al. 2000; Borkowski et al. 2001).

The *upper* limit of the shock temperature and the lower limit to the remnant age are not well constrained by the SEDOV fits, consistent with the expectations for young supernova remnants (Borkowski et al. 2001; Vink 2012). This is due to (a) the uncertainty introduced by the residual contribution from the dust scattering spectrum, (b) the dominant contribution of the diffuse particle background above energies of 6 keV, and (c) the low effective area of the *Chandra* mirrors above 3 keV, with very few sources counts in the 3-6 keV range. These sources of uncertainty are fully reflected in the confidence intervals plotted in Fig. 7 and quoted in the text.

More importantly, however, the fit provides a robust three-sigma *lower* limit of $T_s > 0.3 \text{ keV}$ on the shock temperature. Given the nominal source distance of $D = 8 d_8 \text{ kpc}$ and a measured shock radius of $R \sim 150 \text{ arcsec}$ in the northern hemisphere of the remnant, this lower limit on the shock temperature translates into a three sigma upper limit of $t < 4,600 d_8 \text{ yrs}$ on the age of the remnant. This result is insensitive to the specific shock model used: fits with SEDOV, NEI, PSHOCK, NPSHOCK or even equilibrium (APEC) models yield the same limit.

We determine the mean ambient Hydrogen density n_0 from the ionization age parameter $\tau \equiv n_e t = 4.8 n_0 t$ (for cosmic abundance plasma and standard strong-shock Rankine-Hugoniot jump conditions for a $\gamma = 5/3$ ideal gas, where n_e is the post-shock electron density Safi-Harb et al. 2000) to be $n_0 \approx 0.27^{+0.60}_{-0.05} d_8^{-1} \text{ cm}^{-3}$. The low external density estimate from the ionization age is roughly consistent with estimates derived from the emission measure, $n_{0,EM} \approx 0.16^{+0.22}_{-0.11} d_8^{-1/2} f^{-1/2} \text{ cm}^{-3}$, where $f \leq 1$ is the filling factor of the emitting gas.

The Sedov estimate of the total energy in the blast wave is $E_s \sim 0.09^{+2.2}_{-0.03} \times 10^{51} d_8^2 \text{ ergs}$. Within the uncertainties, this is consistent with typical supernova remnant energies of $E \sim 10^{51} \text{ ergs}$.

From the spectral fits, we find that the abundance of heavy elements in the outer remnant is $Z = 1.3^{+0.9}_{-0.5} Z_{\odot}$ relative to solar, which is consistent with emission predominantly from the forward shock into relatively unenriched material. Because of the possible contamination of the inner remnant by dust scattering emission, we cannot reliably test for enriched emission by the supernova

ejecta.

3. DISCUSSION AND CONCLUSIONS

The upper limit of $t < 4,600 d_8$ years on the age of the remnant makes Circinus X-1 the youngest known X-ray binary. The black hole candidate SS433, the only other firmly established¹⁴ Galactic X-ray binary within a supernova remnant (Geldzahler et al. 1980), has an estimated age of $10^4 \text{ yrs} < t \lesssim 10^5 \text{ yrs}$ (Lockman et al. 2007; Goodall et al. 2011). Two other plausible HMXB candidates in nearby galaxies have been suggested to reside within supernova remnants, the Be/X-ray binary pulsar SXP 1062 (Hénault-Brunet et al. 2012) in the Small Magellanic Cloud, and DEM L241 (Seward et al. 2012) in the Large Magellanic Cloud, both of which were estimated to be of similar age to SS433.

A number of important conclusions follow from this discovery.

If the neutron star formed through core collapse of a massive star then the very young age of the system implies that the companion star cannot be a low mass star, given the orbital constraints derived by Jonker et al. (2007), because a low mass star would not have had time to evolve off the main sequence to fill its Roche lobe at periastron. A massive companion star, most likely an A0 to B5 type supergiant (Jonker et al. 2007), would be consistent with the young age.

The young age of the system explains the high eccentricity and the short orbital evolution time, between $P/\dot{P} \sim 3,000$ years inferred from X-ray dip timing (Parkinson et al. 2003; Clarkson et al. 2004) and $P/\dot{P} \sim 20,000$ years from radio flare timing (Nicolson 2007), since the system has not had time to tidally circularize its orbit from the eccentricity it received in the supernova explosion.

Because the system is so young, the current orbital parameters are likely close to the orbit of the binary immediately after the supernova explosion. The orbital period of $P = 16.5$ days and the eccentricity of $e \sim 0.45$ (Jonker et al. 2007) fall into the expected range of orbital parameters for post supernova HMXBs with kick velocities of several hundred km/s. In systems like this, the neutron star spin, the companion spin, and the orbital axis are likely mutually misaligned (Brandt & Podsiadlowski 1995). Spin-orbit coupling effects can cause precession of the binary orbit and the neutron star spin relative to each other and to the spin of the companion star, consistent with suggestions of precession of the jet axis based on radio (Calvelo et al. 2012a) and X-ray data (Sell et al. 2010). Such precession may induce changes in the accretion geometry that could help explain the strong long term modulation of the X-ray lightcurve (Brandt & Podsiadlowski 1995).

While we consider a core collapse supernova the most likely explanation for the formation of Circinus X-1, a proposed alternative channel for neutron star formation is the accretion-induced collapse (AIC) of a white dwarf (e.g., Canal & Schatzman 1976; Nomoto et al. 1979; Michel 1987; Bhattacharya & van den Heuvel 1991). In

¹⁴ The nature of the central source in the young supernova remnant RCW103 is currently uncertain (Li 2007), but it could be a low-mass X-ray binary at an age similar to Circinus X-1 (De Luca et al. 2006).

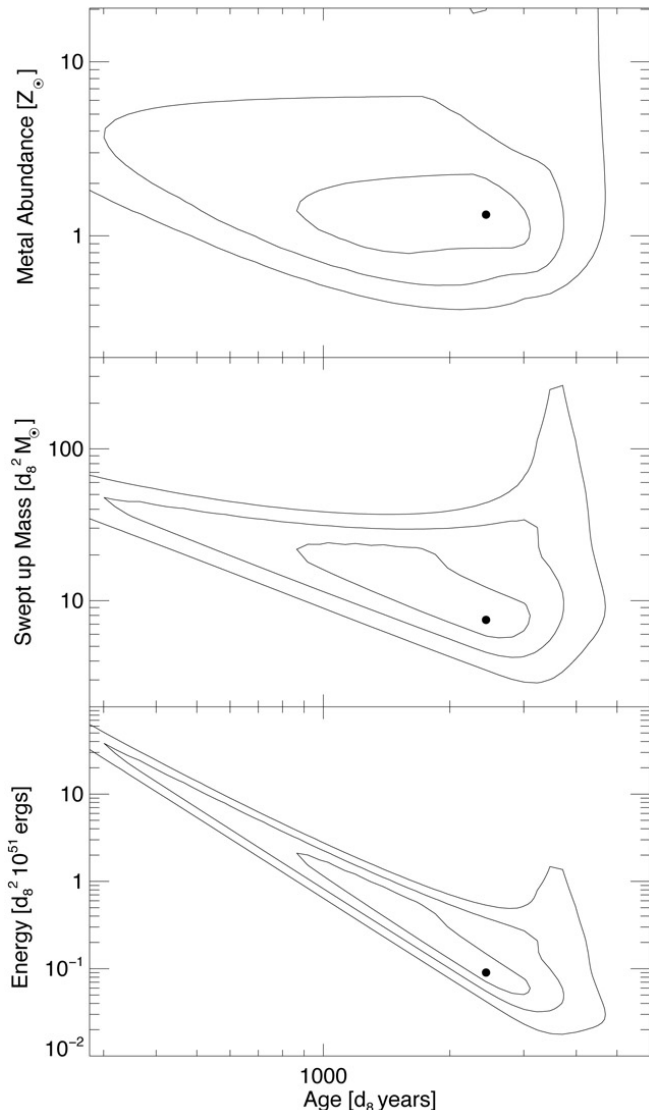


FIG. 7.— Confidence intervals from the SEDOV model fits for the remnant age in years (horizontal axis), the supernova energy in units of 10^{51} ergs, the swept up mass in units of solar masses, and the metal abundance relative to solar values (bottom, middle, and top panel, respectively). From inside out, the contours show the one (68%), two (95%), and three-sigma (99.7%) confidence ranges. The fits provide robust upper limits on the remnant age and lower limits on the swept up mass and supernova energy. The formal best fit parameters are marked by black dots.

this case, the companion would most likely be an evolved low mass star (likely of mass $M \approx 0.4 M_{\odot}$; Jonker et al. 2007). Given the uncertainties in the supernova parameters and the current lack of a firm theoretical understanding of the observational signatures of AIC supernova remnants, we cannot rule out or confirm AIC as a formation scenario.

However, the rapid current orbital evolution of the system, with an orbital time scale of the order of a few thousand years, and the high orbital eccentricity, are hard to understand if the neutron star had formed through AIC: Given that AIC supernovae are generally not believed to impart significant eccentricity to post-supernova binary orbits (Podsiadlowski et al. 2004; Tauris et al. 2013), the current orbital parameters would reflect the pre-

supernova orbit in this scenario. The progenitor white dwarf would have had to accrete of order $0.3 M_{\odot}$ from its companion on time scales much longer than the current orbital evolution time, and the orbit would have circularized.

At an estimated un-absorbed 0.5-10 keV surface brightness of $\Sigma_{0.5,10} \sim 3.5_{-0.8}^{+1.2} \times 10^{-16} \text{ ergs s}^{-1} \text{ cm}^{-2} \text{ arcsec}^{-2}$ (averaged over the spectral extraction region), the remnant has relatively low surface brightness compared to other remnants of similar physical size, comparable to SN 1006, though not as faint as plerionic supernova remnants like G21.5-0.9 (Bocchino et al. 2005; Matheson & Safi-Harb 2010). The low surface brightness likely indicates that the supernova exploded into a low density wind driven by the progenitor star (Dwarkadas 2005; Chevalier 2005), consistent with the low ambient Hydrogen density estimate of $n_0 \approx 0.27_{-0.05}^{+0.60} d_8^{-1} \text{ cm}^{-3}$ inferred from the spectral fits. In this case, the age derived from the SEDOV fits would likely be an overestimate (Dwarkadas 2005).

The estimated swept up mass is $M_s \approx 7.4_{-1.5}^{+16.5} d_8^2 M_{\odot}$, suggesting that the remnant has only recently entered the Sedov phase, where the swept up mass exceeds the ejecta mass. If the remnant is still expanding into the stellar wind bubble blown by its progenitor, we can place a rough lower limit on the progenitor mass of $M_{\text{prog}} = M_{\text{ejecta}} + M_{\text{wind}} + M_{\text{NS}} \gtrsim 7 M_{\odot}$. The low ambient density and the roughly solar metallicity of the emitting gas would be consistent with a type IIP supernova explosion of a progenitor star of mass $M \sim 8$ to $25 M_{\odot}$ (Chevalier 2005).

Based on the evidence that the X-ray nebula is the supernova remnant of Circinus X-1, we conclude that the radio nebula surrounding Circinus X-1 is most likely not inflated by the radio jets of the source, but created through synchrotron emission from standard non-thermal acceleration of electrons in the external shock, as first suggested by Clarkson et al. (2004). The limb-brightened appearance of the radio nebula in Fig. 4 and the filamentary edge of the nebula visible in Fig. 7 of Calvelo et al. (2012b), typical for supernova remnants, is inconsistent with the traditional interpretation of the nebula as a radio lobe. While a jet-inflated bubble of relativistic plasma could conceivably produce a similar external shock in both non-thermal radio and thermal X-ray emission, effectively mimicking a supernova remnant in appearance, the synchrotron emission from within the bubble required to drive such a powerful shock would be five orders of magnitude brighter than the observed radio flux from the entire nebula (Tudose et al. 2006), ruling out the possibility that the large scale nebula is jet powered.

The synchrotron age of $t_{\text{jet}} \sim 1,600$ years inferred for the X-ray jets (Sell et al. 2010) implies that the jets, and thus accretion, must have turned on soon after the explosion. The location of the synchrotron X-ray shock about a third of the way across the remnant might indicate the location where the jets impact the inner edge of the supernova ejecta. The fact that both SS433 and Circinus X-1 exhibit extended synchrotron jet emission suggests that the high-pressure environment of the interior of a supernova remnant boosts synchrotron emission

by confining the relativistic plasma at high pressure.

The asymmetric shape of the radio nebula is more pronounced than in other remnants of core collapse supernovae, with an aspect ratio of more than 2:1 in the North-South vs. East-West direction. This may be a result of an asymmetric explosion and/or a highly anisotropic external medium shaped by the progenitor wind; winds from evolved massive stars in binary systems are known to be highly anisotropic. It is also possible that the Southern protrusion is at least in part caused by energy injection from the jets. This would imply a jet power in excess of 10^{39} ergs s^{-1} , significantly larger than the Eddington luminosity for a neutron star, but similar to the jet power of SS433. Given the similarities in the shapes of the supernova remnants and in the properties of their relativistic jets, Circinus X-1 may present an earlier evolutionary stage of an SS433-like system.

The high visible extinction towards Circinus X-1 explains why the remnant has not been found in narrow-band visible images of the region. However, the supernova itself would have been visible to the naked eye from latitudes lower than about 35 degrees North.

Finally, the very active ongoing accretion from the companion star, the lack of X-ray pulses, and the observed type I X-ray thermonuclear bursts of the source (Tennant et al. 1986; Linares et al. 2010) imply that the surface magnetic field of the neutron star is low, $B \ll 10^{12}$ G (Fujimoto et al. 1981; Bildsten 1998). Any initially high magnetic field cannot have decayed by diffusion alone in the short time since the supernova (e.g., Goldreich & Reisenegger 1992; Harding & Lai 2006). Thus, the neutron star must either have been born with

low magnetic field (possibly by burial through massive fall-back accretion; Muslimov & Page 1995; Ho 2011; Bernal et al. 2013, or if the neutron star formed through accretion-induced collapse of a low-field white dwarf; Bhattacharya & van den Heuvel 1991) or the field must have been buried by the rapid accretion near the Eddington rate (Cumming et al. 2001; Payne & Melatos 2006, 2007) that the source has experienced in the recent past. Given the low magnetic field strength and the implied low rate of magnetic braking, the neutron star is likely spinning at close to the rotation rate it had at birth.

The discovery of the supernova remnant of Circinus X-1 opens a new window on the study of young X-ray binaries. The ability to correlate the rapid, non-linear evolution of the orbital parameters with the accretion behavior of the source holds significant promise for a detailed understanding of the complex, sometimes puzzling behavior of a newly formed X-ray binary.

We would like to thank Jay Gallagher, Ellen Zweibel, and Snezana Stanimirovic for helpful discussions. S.H. and P.S. acknowledge support through CXC grant G09-0056X and NSF grant AST-0908690; W.N.B. acknowledges support through NASA ADP grant NNX10AC99G and CXC contract SV4-74018. This research has made use of data obtained from the Chandra Data Archive and the Chandra Source Catalog, and software provided by the Chandra X-ray Center (CXC) in the application packages included in CIAO. The Australia Telescope Compact Array is part of the Australia Telescope National Facility which is funded by the Commonwealth of Australia for operation as a National Facility managed by CSIRO.

REFERENCES

- Bernal, C. G., Page, D., & Lee, W. H. 2013, *ApJ*, 770, 106
 Bhattacharya, D. & van den Heuvel, E. P. J. 1991, *Phys. Rep.*, 203, 1
 Bildsten, L. 1998, in *NATO ASIC Proc. 515: The Many Faces of Neutron Stars.*, ed. R. Buccheri, J. van Paradijs, & A. Alpar, 419
 Bocchino, F., van der Swaluw, E., Chevalier, R., & Bandiera, R. 2005, *A&A*, 442, 539
 Borkowski, K. J., Lyerly, W. J., & Reynolds, S. P. 2001, *ApJ*, 548, 820
 Brandt, N. & Podsiadlowski, P. 1995, *MNRAS*, 274, 461
 Calvelo, D. E., Fender, R. P., Tzioumis, A. K., & Broderick, J. W. 2012a, *MNRAS*, 419, L54
 Calvelo, D. E., Fender, R. P., Tzioumis, A. K., Kawai, N., Broderick, J. W., & Bell, M. E. 2012b, *MNRAS*, 419, 436
 Canal, R. & Schatzman, E. 1976, *A&A*, 46, 229
 Chevalier, R. A. 2005, *ApJ*, 619, 839
 Clarkson, W. I., Charles, P. A., & Onyett, N. 2004, *MNRAS*, 348, 458
 Cumming, A., Zweibel, E., & Bildsten, L. 2001, *ApJ*, 557, 958
 De Luca, A., Caraveo, P. A., Mereghetti, S., Tiengo, A., & Bignami, G. F. 2006, *Science*, 313, 814
 Diehl, S. & Statler, T. S. 2006, *MNRAS*, 368, 497
 Dwarkadas, V. V. 2005, *ApJ*, 630, 892
 Fujimoto, M. Y., Hanawa, T., & Miyaji, S. 1981, *ApJ*, 247, 267
 Geldzahler, B. J., Pauls, T., & Salter, C. J. 1980, *A&A*, 84, 237
 Goldreich, P. & Reisenegger, A. 1992, *ApJ*, 395, 250
 Goodall, P. T., Alouani-Bibi, F., & Blundell, K. M. 2011, *MNRAS*, 414, 2838
 Hamilton, A. J. S., Sarazin, C. L., & Chevalier, R. A. 1983, *ApJS*, 51, 115
 Harding, A. K. & Lai, D. 2006, *Reports on Progress in Physics*, 69, 2631
 Heinz, S., Schulz, N. S., Brandt, W. N., & Galloway, D. K. 2007, *ApJ*, 663, L93
 Hénault-Brunet, V., Oskinova, L. M., Guerrero, M. A., Sun, W., Chu, Y.-H., Evans, C. J., Gallagher, III, J. S., Gruendl, R. A., & Reyes-Iturbide, J. 2012, *MNRAS*, 420, L13
 Ho, W. C. G. 2011, *MNRAS*, 414, 2567
 Högbom, J. A. 1974, *A&AS*, 15, 417
 Iaria, R., Spanò, M., Di Salvo, T., Robba, N. R., Burderi, L., Fender, R., van der Klis, M., & Frontera, F. 2005, *ApJ*, 619, 503
 Jonker, P. G. & Nelemans, G. 2004, *MNRAS*, 354, 355
 Jonker, P. G., Nelemans, G., & Bassa, C. G. 2007, *MNRAS*, 374, 999
 Li, X.-D. 2007, *ApJ*, 666, L81
 Linares, M., Watts, A., Altamirano, D., Soleri, P., Degenaar, N., Yang, Y., Wijnands, R., Casella, P., Homan, J., Chakrabarty, D., Rea, N., Armas-Padilla, M., Cavecchi, Y., Kalamkar, M., Kaur, R., Patruno, A., & van der Klis, M. 2010, *ApJ*, 719, L84
 Lockman, F. J., Blundell, K. M., & Goss, W. M. 2007, *MNRAS*, 381, 881
 Matheson, H. & Safi-Harb, S. 2010, *ApJ*, 724, 572
 Michel, F. C. 1987, *Nature*, 329, 310
 Muslimov, A. & Page, D. 1995, *ApJ*, 440, L77
 Nicolson, G. D. 2007, *The Astronomer's Telegram*, 985, 1
 Nomoto, K., Miyaji, S., Sugimoto, D., & Yokoi, K. 1979, in *IAU Colloq. 53: White Dwarfs and Variable Degenerate Stars*, ed. H. M. van Horn & V. Weidemann, 56–60
 Oosterbroek, T., van der Klis, M., Kuulkers, E., van Paradijs, J., & Lewin, W. H. G. 1995, *A&A*, 297, 141
 Parkinson, P. M. S., Tournear, D. M., Bloom, E. D., Focke, W. B., Reilly, K. T., Wood, K. S., Ray, P. S., Wolff, M. T., & Scargle, J. D. 2003, *ApJ*, 595, 333
 Payne, D. J. B. & Melatos, A. 2006, *ApJ*, 652, 597
 —. 2007, *MNRAS*, 376, 609

- Podsiadlowski, P., Langer, N., Poelarends, A. J. T., Rappaport, S., Heger, A., & Pfahl, E. 2004, *ApJ*, 612, 1044
- Predehl, P. & Klose, S. 1996, *A&A*, 306, 283
- Predehl, P. & Schmitt, J. H. M. M. 1995, *A&A*, 293, 889
- Safi-Harb, S., Petre, R., Arnaud, K. A., Keohane, J. W., Borkowski, K. J., Dyer, K. K., Reynolds, S. P., & Hughes, J. P. 2000, *ApJ*, 545, 922
- Sault, R. J., Teuben, P. J., & Wright, M. C. H. 1995, in *Astronomical Society of the Pacific Conference Series, Vol. 77, Astronomical Data Analysis Software and Systems IV*, ed. R. A. Shaw, H. E. Payne, & J. J. E. Hayes, 433
- Sault, R. J. & Wieringa, M. H. 1994, *A&AS*, 108, 585
- Sell, P. H., Heinz, S., Calvelo, D. E., Tudose, V., Soleri, P., Fender, R. P., Jonker, P. G., Schulz, N. S., Brandt, W. N., Nowak, M. A., Wijnands, R., van der Klis, M., & Casella, P. 2010, *ApJ*, 719, L194
- Seward, F. D., Charles, P. A., Foster, D. L., Dickel, J. R., Romero, P. S., Edwards, Z. I., Perry, M., & Williams, R. M. 2012, *ApJ*, 759, 123
- Soleri, P., Heinz, S., Fender, R., Wijnands, R., Tudose, V., Altamirano, D., Jonker, P. G., van der Klis, M., Kuiper, L., Kaiser, C., & Casella, P. 2009, *MNRAS*, 397, L1
- Stewart, R. T., Caswell, J. L., Haynes, R. F., & Nelson, G. J. 1993, *MNRAS*, 261, 593
- Tauris, T. M., Sanyal, D., Yoon, S.-C., & Langer, N. 2013, *A&A*, 558, A39
- Tennant, A. F., Fabian, A. C., & Shafer, R. A. 1986, *MNRAS*, 221, 27P
- Tudose, V., Fender, R. P., Kaiser, C. R., Tzioumis, A. K., van der Klis, M., & Spencer, R. E. 2006, *MNRAS*, 372, 417
- Vink, J. 2012, *A&A Rev.*, 20, 49